Available online at www.sciencedirect.com

ScienceDirect

Advances in Space Research 63 (2019) 3223–3234

ADVANCES IN SPACE RESEARCH (a COSPAR publication)

www.elsevier.com/locate/asr

Optimal guidance and collision avoidance for docking with the rotating target spacecraft

Zheyao Xu [a,*], Yukun Chen [b], Zhexuan Xu [c]

[a] Beijing Institute of Astronautical Systems Engineering, Beijing 100076, People's Republic of China
[b] CASIC Space Engineering Development Co. Ltd, Beijing 100039, People's Republic of China
[c] State Key Laboratory of Engine, Tianjin University, Tianjin 300072, People's Republic of China

Received 12 August 2018; received in revised form 15 January 2019; accepted 17 January 2019
Available online 28 January 2019

Abstract

The guidance and control strategy for spacecraft rendezvous and docking are of vital importance, especially for a chaser spacecraft docking with a rotating target spacecraft. Approach guidance for docking maneuver in planar is studied in this paper. Approach maneuver includes two processes: optimal energy approach and the following flying-around approach. Flying-around approach method is presented to maintain a fixed relative distance and attitude for chaser spacecraft docking with target spacecraft. Due to the disadvantage of energy consumption and initial velocity condition, optimal energy guidance is presented and can be used for providing an initial state of flying-around approach process. The analytical expression of optimal energy guidance is obtained based on the Pontryagin minimum principle which can be used in real time. A couple of solar panels on the target spacecraft are considered as obstacles during proximity maneuvers, so secure docking region is discussed. A two-phase optimal guidance method is adopted for collision avoidance with solar panels. Simulation demonstrates that the closed-loop optimal energy guidance satisfies the ending docking constraints, avoids collision with time-varying rotating target, and provides the initial velocity conditions of flying-around approach maneuver. Flying-around approach maneuver can maintain fixed relative position and attitude for docking.

Keywords: Optimal guidance; Collision avoidance; Docking; Rotating target spacecraft

1. Introduction

Rendezvous and proximity maneuvers are precondition for orbital assembly, repairing broken satellite, on-orbit servicing (Wu et al., 2018), and debris removal missions (Hakima et al., 2018). For formation flight, rendezvous, proximity maneuvers or docking, theoretical and experimental research has already developed (Scharf et al., 2010a, 2010b). Two 3-DOF spacecraft simulators are used to test the autonomous approach and docking between a chaser spacecraft and a collaborative target spacecraft (Romano et al., 2007). Collision avoidance technology is of vital importance to formation control; reconfiguration and docking. MIT Space Systems Laboratory verified collision avoidance method on SPHERES testbed (Mohan et al., 2007; Nolet and Miller, 2007). In the experiments, the autonomous distributed multiple spacecraft close-proximity control algorithm is a combination of Linear Quadratic Regulator (LQR) and artificial potential field (APF) control algorithms (McCamish et al., 2009). Resource Aggregated Reconfigurable Control was tested on the SPHERES with avoiding obstacles in reference (Jewison et al., 2014). For docking maneuvers, references (Ciarcià et al., 2014; Ciarcià and Romano, 2012) give sub-

* Corresponding author.
E-mail address: xzydtc@126.com (Z. Xu).

https://doi.org/10.1016/j.asr.2019.01.026
0273-1177/

optimal guidance strategy through solving inverse dynamics and nonlinear programming problem.

Bevilacqua adopted four 3-DOF spacecraft simulators to study the navigation and control algorithm for multiple spacecraft autonomous maneuvers (Bevilacqua et al., 2009; Pellegrini et al., 2010). Reference (Bevilacqua et al., 2009) gave sub-optimal attitude and position control method for multiple spacecraft assembly using a Linear Quadratic Regulator (LQR), and presented the control method of the assembled spacecraft simulator. Reference (Curti et al., 2010) introduced the tracking of linear dynamic models control method for spacecraft rotation and translation. Bevilacqua introduced a control algorithm for close proximity multiple spacecraft autonomous maneuvers and collision avoidance, which is based on hybrid LQR and artificial potential function (APF) (Bevilacqua et al., 2011). Through a decisional logic, this algorithm overcame the problem of local minima. The weighting matrices are changed as the spacecraft's position changes to avoid the influence of the high tracking error at the beginning of the maneuver. However, some noncooperative targets may have a rotating motion. Proximity maneuvers for the rotating target need to take into account the rotating docking position and collision avoidance. The control problem cannot be described as a simple linear system, so LQR algorithm is not suitable for this situation.

To rendezvous with a tumbling satellite, references (Sun and Zheng, 2017) given a relative motion control method for parametric uncertainties problem, but the optimization problem and collision avoidance are not considered. Ma Z studied the optimal control problem of chaser spacecraft approaching the target in the plane (Ma et al., 2006). The minimum-time and minimum-energy rendezvous are discussed and numerical solution is calculated by iterations. However the iteration process costs time and collision avoidance is not considered. Reference (Boyarko et al., 2011) developed a 6-DOF relative motion model of target-chaser rendezvous. The optimal control problem of minimum time and minimum energy are solved numerically by using the Gauss pseudospectral approach. A path constraint for collision avoidance with the target body is imposed. Trajectory planning algorithm for collision avoidance with tumbling target using the Gauss pseudospectral method is given in reference (Chu et al., 2016). And a closed-loop control is used to track the optimised trajectory. These methods also need long computational time. To reduce the computational complexity and obtain rapid optimization; Sternberg and Miller use reduced parameterization method to avoid a full optimization (Sternberg, 2017, 2018; Sternberg and Miller, 2018), and Matlab's fmincon function is used to solve the optimization problem. To the spacecraft on the orbit, analytical expression should be investigated for real time operations. However, an analytical expression for rotation target docking is still a problem need to be studied now.

Experimental research of planar docking with a rotating target is executed in reference (Wilde et al., 2016). The control forces and torque are obtained by an inverse dynamics operation of preassigned trajectory. The docking maneuver is divided into the free-flight phase and the final docking approach phase. The closed-loop iterative method by measuring and updating the state of the target is adopted. Similarly, an Archimedes Spiral rendezvous approach path is researched in reference (Sternberg and Miller, 2017).

However, the inverse dynamics solver and Archimedes Spiral method may not be optimal. And the collision avoidance with solar panels still need be considered. Guidance algorithm for planar docking with rotating target is presented in this paper. Analytical expression of rotation target docking guidance is one of the main purposes in this paper. The docking process is divided into two processes: optimal energy approach and flying-around approach. Collision avoidance with solar panels is considered in these two processes. In Section 2, flying-around approach method is discussed firstly. Because long relative distance may lead to high energy consumption in flying-around approach, optimal energy guidance method is presented in Section 3. Optimal energy approach is executed before flying-around approach, and used to provide a suitable initial condition for following flying-around approach. The dynamics of relative motion with rotation is modeled. The analytical expression of minimum energy guidance is solved based on the Pontryagin minimum principle. Secure docking region and two phases of optimal trajectory for collision avoidance are discussed. The simulations are given in Section 4.

2. Flying-around approach method

In this section, the relative motion guidance in target coordinate system is discussed firstly. Then an inverse rotational dynamics process is adopted to obtain the guidance law of absolute motion. The chaser spacecraft and the target spacecraft are shown in Fig. 1. In the initial time, the chaser spacecraft has a very short distance (about tens of meters to several meters) from the target spacecraft, waiting for docking. The target spacecraft rotates on the orbit. This paper makes an assumption that the chaser spacecraft has already known the target spacecraft's motion by estimation algorithm, including the target's relative position,

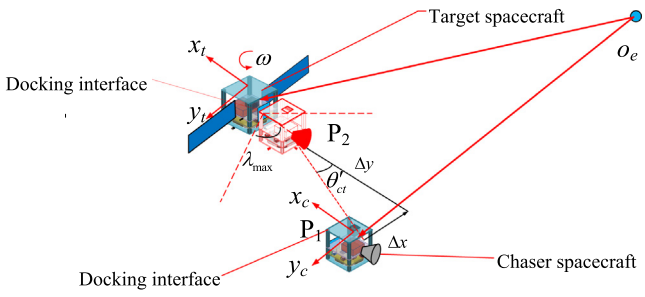

Fig. 1. Chaser and target spacecraft.

relative angle, relative velocity, relative angle velocity. And the suitable docking interface of the target is determined for chaser before docking. The thrust of chaser spacecraft can be adjusted by PWM method or flow control method. When rotation angular velocity of target spacecraft is perpendicular to docking axis, the chaser spacecraft must fly around the target during docking. However, when rotation angular velocity is parallel to the docking axis, chaser just need rotate synchronously as the target during docking. In fact, angular velocity can always be decomposed into two components that are parallel to docking axis and perpendicular to the docking axis. The rotation motion can be regarded as the combination of the two kind of motion. This paper mainly considers the complicated problem of docking caused by the component of rotation angular velocity of target perpendicular to docking axis. A more difficult situation for docking is assumed that the target has a pair of solar panels which are also perpendicular to the rotation angular velocity, as shown in Fig. 1. When target rotates, the solar panels on it will be regarded as obstacles. After starting the docking maneuver, chaser spacecraft should approach the target spacecraft and avoid colliding with the solar panels. When chaser spacecraft enters the docking position as the red spacecraft shown in Fig. 1, chaser should maintain the relative distance and attitude from the target, to provide a suitable docking condition.

For a rotating target, the chaser spacecraft must move around the target to provide a constant relative position at the end of the docking process. So the relative motion is discussed firstly. The chaser and target body-fixed coordinate system $o_c x_c y_c z_c$ and $o_t x_t y_t z_t$ are defined, as shown in Fig. 1. The origin o_c and o_t are the center of chaser and target. The docking interface of chaser points to the x_c and that of target points to the $-x_t$. The initial relative position and relative angle from chaser to target are Δx, Δy and θ_{ct}. Chaser spacecraft translates from initial position P_1 to the target position P_2. Simultaneously, chaser spacecraft rotates a relative angle θ_{ct}. Then the chaser spacecraft maintains the relative position and angle, and docks with the target spacecraft. At the end of the proximity maneuvers, the relative velocity and relative angle velocity are zero.

A control strategy for relative position and angle (Δx, Δy and θ_{ct}) in the $o_t x_t y_t z_t$ is adopted, which includes 'acceleration-constant velocity-deceleration (ACD)', 'acceleration-deceleration (AD)' and 'deceleration motion (DM)'. The relative acceleration in direction x_t and y_t, and relative angular acceleration in $o_t x_t y_t z_t$ can be obtained by Eqs. (32)–(35) in the Appendix A. In the end of the relative motion, the relative velocity is zero by Eqs. (32)–(35). During the maneuver, to avoid colliding with the solar panels, a secure range is defined. $\lambda_{\max}$ depends on the docking mechanism and the physical geometry of the two spacecraft, usually $\lambda_{\max} < 90°$. The secure angle $\lambda_{\max}$ is shown in Fig. 1. In the initial time, the angle θ'_{ct} must be smaller than the limited secure angle $\lambda_{\max}$, $-\lambda_{\max} \leqslant \theta'_{ct} \leqslant \lambda_{\max}$. This is initial condition of secure docking of flying-around approach method.

When target spacecraft rotates, chaser spacecraft circles around target spacecraft synchronously. $\delta \boldsymbol{r}$ is the displacement vectors from chaser spacecraft to target spacecraft. The acceleration of chaser spacecraft $\ddot{\boldsymbol{R}}_{o_e c}$ is

$$\ddot{\boldsymbol{R}}_{o_e c} = \ddot{\boldsymbol{R}}_{o_e t} - \frac{d^2 \delta \boldsymbol{r}}{dt^2} \tag{1}$$

where $\ddot{\boldsymbol{R}}_{o_e t}$ is the target acceleration, $\frac{d^2 \delta \boldsymbol{r}}{dt^2}$ is the relative acceleration as Eq. (2). The acceleration of chaser and target include the acceleration of gravity and thrust. To the rendezvous and docking of two spacecraft in a short distance, the high order items in relative orbital dynamics can be considered as a little disturbance and the disturbance can be compensated by controller. So the influence of gravity and high order items of angular velocity in relative movement can be ignored.

$$\frac{d^2 \delta \boldsymbol{r}}{dt^2} = \delta \ddot{\boldsymbol{r}}^t + 2\boldsymbol{\omega}_t \times \delta \dot{\boldsymbol{r}}^t + \boldsymbol{\omega}_t \times (\boldsymbol{\omega}_t \times \delta \boldsymbol{r}^t) + \dot{\boldsymbol{\omega}}_t \times \delta \boldsymbol{r}^t \tag{2}$$

In Eq. (2), $\delta \ddot{\boldsymbol{r}}^t = \boldsymbol{a}(t)$ is the relative acceleration in $o_t x_t y_t z_t$ which can be calculated by Eqs. (32)–(35). $\boldsymbol{\omega}_t$ is the angular velocity of target spacecraft. The relative motion orbital coordinate system $o_o x_o y_o z_o$ (the z_o axis is parallel to the rotation axis) at the initial docking time is used as reference coordinate system. The rotation angle between the coordinate system $o_t x_t y_t z_t$ and $o_o x_o y_o z_o$ is θ. The rotation matrix is given as Eq. (3).

$$C_{ot} = \begin{bmatrix} \cos\theta & \sin\theta & 0 \\ -\sin\theta & \cos\theta & 0 \\ 0 & 0 & 1 \end{bmatrix} \tag{3}$$

Relative velocity $\frac{d\delta \boldsymbol{r}}{dt}$ in target spacecraft body-fixed coordinate system is

$$\frac{d\delta \boldsymbol{r}}{dt} = \delta \dot{\boldsymbol{r}}^t + \boldsymbol{\omega}_t \times \delta \boldsymbol{r}^t \tag{4}$$

Then, the velocity of chaser spacecraft in the orbital coordinate system $o_o x_o y_o z_o$ can be obtained as Eq. (5).

$$\dot{\boldsymbol{R}}^o_{o_o c} = \dot{\boldsymbol{R}}^o_{o_o t} - C_{ot} \frac{d\delta \boldsymbol{r}}{dt} \tag{5}$$

The relative motion trajectory can also be described in the orbital coordinate system $o_o x_o y_o z_o$. The point (x^t, y^t, z^t) on the relative motion trajectory in coordinate system $o_t x_t y_t z_t$ is converted to the point (x^o, y^o, z^o) in the orbital coordinate system as Eq. (6).

$$\begin{bmatrix} x^o \\ y^o \\ z^o \end{bmatrix} = C_{ot} \begin{bmatrix} x^t \\ y^t \\ z^t \end{bmatrix} + \begin{bmatrix} O^t_x \\ O^t_y \\ O^t_z \end{bmatrix} \tag{6}$$

where $\left[O^t_x, O^t_y, O^t_z\right]$ is the location of the origin of coordinate system $o_t x_t y_t z_t$ in $o_o x_o y_o z_o$. During the proximity

maneuvers, the relative angle θ_{tc} changes simultaneously. The angle θ_{tc} satisfies

$$\dot{\theta}_{tc} = -\omega_t + \omega_c \tag{7}$$

The relative angle θ_{tc} should equal to zero to keep the docking axes of the two spacecraft aligned. So the relative angle is adjusted by attitude control system. The relative angular velocity $\dot{\theta}_{tc}$ control strategy is also 'ACD',' AD' and 'DM'. Then the expected angular velocity of chaser is obtained by $\omega_c = \omega_t + \dot{\theta}_{tc}$. After θ_{ct} is controlled to zero, the chaser spacecraft should maintain rotating synchronously with target spacecraft, that is $\omega_c = \omega_t$, and keep $\theta_{tc} = 0$ for docking. The proximity accelerations in the orbital coordinate system are obtained by Eqs. (1), (2) and the relative acceleration (32)–(35), which is calculated based on the initial relative position and given reference relative acceleration a_r. The position, velocity and angular velocity of target spacecraft are variable. The acceleration of chaser can be solved in real time as long as the motion status of target spacecraft can be estimated. So in flying-around approach method, the acceleration $\ddot{\boldsymbol{R}}_{o_c c}$ of closed-loop control form is obtained by the relative acceleration (32)–(35) and the inverse dynamics process (1) and (2).

3. Optimal energy guidance method

3.1. Closed-loop optimal energy guidance method

This section will present an optimal guidance method for approaching rotating target spacecraft. To obtain the analytical expression which can generate real time guidance law, the translation motion is emphatically researched in this section. The rotation control of chaser adopts the method presented in last section. Point A and B are the center of chaser and target. Point C is the positon of A when chaser successes in docking with target (shown as Fig. 2). Point C rotates around point B in angular velocity $\boldsymbol{\omega}_t$. The relative displacement vectors $\boldsymbol{R}_{CA}$ is

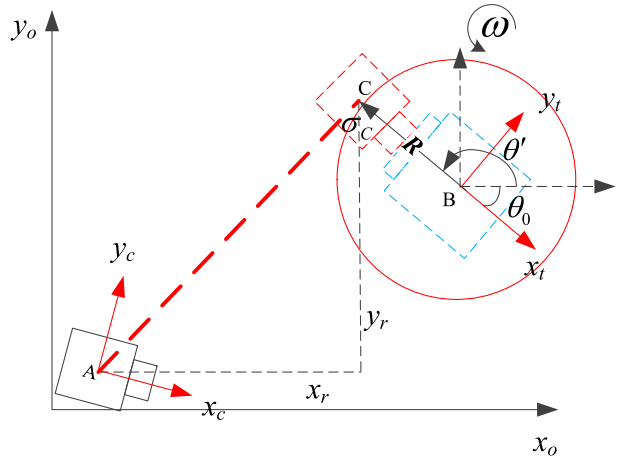

Fig. 2. Schematic of docking dynamics.

$$\boldsymbol{R}_{CA} = \boldsymbol{R}_{O_oC} - \boldsymbol{R}_{O_oA} \tag{8}$$

O_o is the origin of orbital coordinate system at initial docking time. The dynamics of point C satisfies.

$$\begin{aligned} \boldsymbol{R}_{O_oC} &= \boldsymbol{R}_{O_oB} + \boldsymbol{R}_{BC} \\ \boldsymbol{V}_C &= \boldsymbol{V}_t + \boldsymbol{\omega}_t \times \boldsymbol{R}_{BC} \\ \boldsymbol{a}_C &= \dot{\boldsymbol{V}}_t + \boldsymbol{\omega}_t \times (\boldsymbol{\omega}_t \times \boldsymbol{R}_{BC}) + \dot{\boldsymbol{\omega}}_t \times \boldsymbol{R}_{BC} \end{aligned} \tag{9}$$

Then the relative motion dynamics between point C and point A in the orbital coordinate system is described as Eq. (10).

$$\begin{aligned} \dot{x}_r &= V_x^C - V_{cx} \\ \dot{y}_r &= V_y^C - V_{cy} \\ \ddot{x}_r &= -a_{cx} + \dot{V}_{tx} + \omega_t^2 R\cos\theta - \dot{\omega}_t R\sin\theta \\ \ddot{y}_r &= -a_{cy} + \dot{V}_{ty} - \omega_t^2 R\sin\theta - \dot{\omega}_t R\cos\theta \end{aligned} \tag{10}$$

Define the state vector $\boldsymbol{x} = [x_r \quad y_r \quad \dot{x}_r \quad \dot{y}_r]^T$. Accelerations are the control input $a_{cx} = u_x, a_{cy} = u_y$. The state equation is

$$\begin{aligned} \dot{x} = &\begin{bmatrix} 0 & 0 & 1 & 0 \\ 0 & 0 & 0 & 1 \\ \multicolumn{4}{c}{\mathbf{0}_{2\times4}} \end{bmatrix} x + \begin{bmatrix} \multicolumn{4}{c}{\mathbf{0}_{2\times4}} \\ 0 & 0 & -1 & 0 \\ 0 & 0 & 0 & -1 \end{bmatrix} \begin{bmatrix} \mathbf{0}_{2\times1} \\ u_x \\ u_y \end{bmatrix} \\ &+ \begin{bmatrix} \mathbf{0}_{2\times1} \\ \dot{V}_{tx} + \omega_t^2 R\cos\theta - \dot{\omega}_t R\sin\theta \\ \dot{V}_{ty} - \omega_t^2 R\sin\theta - \dot{\omega}_t R\cos\theta \end{bmatrix} \end{aligned} \tag{11}$$

where θ satisfies

$$\begin{aligned} \theta &= -\omega t + \theta_0 \\ \dot{\theta} &= -\omega \end{aligned} \tag{12}$$

The cost function for minimum energy expenditure is

$$J = \frac{1}{2}\int_{t_0}^{t_f} u_x^2 + u_y^2 dt \tag{13}$$

The Hamiltonian function is given by Eq. (14).

$$\begin{aligned} H = &\frac{1}{2}\left(u_x^2 + u_y^2\right) + \lambda_1 x_3 + \lambda_2 x_4 \\ &+ \lambda_3\left(\dot{V}_{tx} + \omega_t^2 R\cos\theta - \dot{\omega}_t R\sin\theta - u_x\right) \\ &+ \lambda_4\left(\dot{V}_{ty} - \omega_t^2 R\sin\theta - \dot{\omega}_t R\cos\theta - u_y\right) \end{aligned} \tag{14}$$

The optimal command can be determined by minimizing the Hamiltonian in Eq. (14), $H^* = \min_{u\in\Omega} H$. The controls are bounded:$-a_{\max} \leqslant u_x, u_y \leqslant a_{\max}$

$$u_x = \begin{cases} a_{\max} & \lambda_3 \geqslant a_{\max} \\ \lambda_3 & a_{\max} < \lambda_3 < a_{\max} \\ -a_{\max} & \lambda_3 \leqslant -a_{\max} \end{cases} \tag{15}$$

$$u_y = \begin{cases} a_{\max} & \lambda_4 \geqslant a_{\max} \\ \lambda_4 & a_{\max} < \lambda_4 < a_{\max} \\ -a_{\max} & \lambda_4 \leqslant -a_{\max} \end{cases} \tag{16}$$

By the adjoint equation $\dot{\lambda} = -\frac{\partial H}{\partial x}$, then

$$\dot{\lambda}_1 = 0 \quad \dot{\lambda}_2 = 0 \quad \dot{\lambda}_3 = -\lambda_1 \quad \dot{\lambda}_4 = -\lambda_2 \tag{17}$$

So co-state λ_1 and λ_2 are constant. The solution of Eq. (17) is

$$\begin{aligned} \lambda_3 &= -\lambda_1(t - c_1) \\ \lambda_4 &= -\lambda_2(t - c_2) \end{aligned} \tag{18}$$

where c_1 and c_2 are constant. A good docking condition is that the target and chaser have zero relative motion. I.e. point C and point A have the same position and velocity at the final time. The goal of the guidance algorithm is to make the two spacecraft zero relative motion. So the terminal condition is $\boldsymbol{x}(t_f) = \mathbf{0}$. Then the kinematics satisfies

$$\begin{aligned} x_r(t) &= R_{O_oBx} + R_{BCx} - R_{O_oAx} = R_{O_oBx} + R\cos\theta' - R_{O_oAx} = 0 \\ y_r(t) &= R_{O_oBy} + R_{BCy} - R_{O_oAy} = R_{O_oBy} + R\sin\theta' - R_{O_oAy} = 0 \\ \dot{x}_r(t) &= V_{tx} - \omega_t R\sin\theta - V_{cx} = 0 \\ \dot{y}_r(t) &= V_{ty} - \omega_t R\cos\theta - V_{cy} = 0 \end{aligned} \tag{19}$$

where θ' is the angle that the axis x_o rotates anticlockwise to vector $\boldsymbol{R}$ (as shown in Fig. 2). Angle θ' satisfies $\theta' = \pi$ - $\theta_0 + \omega t$. The position and velocity of point A at any time t is obtained by integrating the controls.

$$\begin{aligned} V_{cx}(t) &= \int_{t_0}^{t} u_x dt + V_{cx}|_{t_0} = -\lambda_1\left(\frac{t^2}{2} - c_1 t\right) + V_{cx}|_{t_0} \\ V_{cy}(t) &= \int_{t_0}^{t} u_y dt + V_{cy}|_{t_0} = -\lambda_2\left(\frac{t^2}{2} - c_2 t\right) + V_{cy}|_{t_0} \\ R_{O_oAx}(t) &= \int_{t_0}^{t} V_{cx} dt + R_{O_oAx}|_{t_0} = R_{O_oAx}|_{t_0} - \lambda_1\left(\frac{t^3}{6} - c_1\frac{t^2}{2}\right) + V_{cx}t \\ R_{O_oAy}(t) &= \int_{t_0}^{t} V_{cy} dt + R_{O_oAy}|_{t_0} = R_{O_oAy}|_{t_0} - \lambda_2\left(\frac{t^3}{6} - c_2\frac{t^2}{2}\right) + V_{cy}t \end{aligned} \tag{20}$$

By using Eqs. (19) and (20), the terminal conditions becomes

$$\begin{aligned} &R_{O_oBx}|_{t_f} + R\cos(\pi - \theta_0 + \omega t) - R_{O_oAx}|_{t_0} + \lambda_1\left(\frac{t_f^3}{6} - c_1\frac{t_f^2}{2}\right) - V_{cx}|_{t_0}^{t_f} = 0 \\ &R_{O_oBy}|_{t_f} + R\sin(\pi - \theta_0 + \omega t) - R_{O_oAy}|_{t_0} + \lambda_2\left(\frac{t_f^3}{6} - c_2\frac{t_f^2}{2}\right) - V_{cy}|_{t_0}^{t_f} = 0 \\ &V_{tx} - \omega_t R\sin(-\omega t + \theta_0) + \lambda_1\left(\frac{t_f^2}{2} - c_1 t_f\right) - V_{cx}|_{t_0} = 0 \\ &V_{ty} - \omega_t R\cos(-\omega t + \theta_0) + \lambda_2\left(\frac{t_f^2}{2} - c_2 t_f\right) - V_{cy}|_{t_0} = 0 \end{aligned} \tag{21}$$

The parameters λ_1,λ_2,c_1 and c_2 that are the function of the final time t_f can be solved using Eq. (21). Then the closed loop form of the guidance command is discussed below. The optimal guidance is suitable for the situation that rotating target has time-varying angular rate position. At the time $t_i \subset [0, t_f]$, the current state becomes the new initial state. And the final state of target spacecraft is estimated according to current measurements of the state. If the preselected final docking position does not change, the final time t_f is updated according to the rest of rotation angle $\Delta\theta$ and the rotation angular rate ω.

$$t_f(t_i) = \frac{\Delta\theta(t_i)}{\omega(t_i)} \tag{22}$$

The parameters λ_1,λ_2,c_1 and c_2 are updated according to the current state of t_i.

$$\begin{aligned} \lambda_1 = &-(12R_{O_oAx}|_{t_i} - 12R_{O_oBx}|_{t_f} + 6V_{tx}|_{t_f}t_f + V_{cx}|_{t_i}t_f \\ &+ 12R\cos(\omega_t t_f - \theta_0) \\ &- 6\omega_t t_f R\sin(\theta_0 - \omega_t t_f))/t_f^3 \end{aligned} \tag{23}$$

$$\begin{aligned} \lambda_2 = &-(12R_{O_oAy}|_{t_i} - 12R_{O_oBy}|_{t_f} + 6V_{ty}|_{t_f}t_f + V_{cy}|_{t_i}t_f \\ &+ 12R\sin(\omega_t t_f - \theta_0) - 6\omega_t t_f R\cos(\theta_0 - \omega_t t_f))/t_f^3 \end{aligned} \tag{24}$$

$$\begin{aligned} c_1 = &\left(3R_{O_oAx}|_{t_i}t_f - 3R_{O_oBx}|_{t_f}t_f + V_{tx}|_{t_f}t_f^2 + 2V_{cx}|_{t_i}t_f^2\right. \\ &+3Rt_f\cos(\omega_t t_f - \theta_0) - \omega_t t_f^2 R\sin(\theta_0 - \omega_t t_f))/6R_{O_oAx}|_{t_i} \\ &- 6R_{O_oBx}|_{t_f} + 3V_{tx}|_{t_f}t_f + 3V_{cx}|_{t_i}t_f + 6R\cos(\omega_t t_f - \theta_0) \\ &\left.-3\omega_t t_f R\sin(\theta_0 - \omega_t t_f)\right) \end{aligned} \tag{25}$$

$$\begin{aligned} c_2 = &\left(3R_{O_oAy}|_{t_i}t_f - 3R_{O_oBy}|_{t_f}t_f + V_{ty}|_{t_f}t_f^2 + 2V_{cy}|_{t_i}t_f^2\right. \\ &+3Rt_f\cos(\omega_t t_f - \theta_0) - \omega_t t_f^2 R\sin(\theta_0 - \omega_t t_f))/(6R_{O_oAy}|_{t_i} \\ &- 6R_{O_oBy}|_{t_f} + 3V_{ty}|_{t_f}t_f + 3V_{cy}|_{t_i}t_f \\ &\left.+6R\cos(\omega_t t_f - \theta_0) - 3\omega_t t_f R\sin(\theta_0 - \omega_t t_f)\right) \end{aligned} \tag{26}$$

By using Eqs. (15), (16), (18), (23)–(26) and state Eq. (11), the optimal guidance and trajectory can be generated. When chaser spacecraft reaches the terminal potion, point A and point C have the same velocities. The attitude of chaser is also adjusted in the approach process by the method discussed in Section 2. The rotation angle of chaser is obtained based on the target rotation angle θ_{t_f}. From Eqs. (23) and (24) we know, there is a denominator t_f^3 which makes λ_1 and λ_2 singular when t_f approaches to zero (for example $t_f(t_i) = 0.01$). So when chaser is close to docking point C, the flying-around approach method presented in last section will be adopted, and then chaser spacecraft maintains a fixed relative position to dock with target spacecraft.

3.2. Secure docking region

Collisions avoidance between chaser spacecraft and target spacecraft must be considered. A secure docking region is discussed below. Two lines that cross point A and are tangent to the circle trajectory of point C is shown in Fig. 3. The two points of tangency separate the circle into two arcs. The arc near the point A (the red circle in Fig. 3) is the front docking region. The other is the back docking region (the blue circle in Fig. 3). When the preselected docking point is in the front docking region, docking trajectory does not come across the circle trajectory because

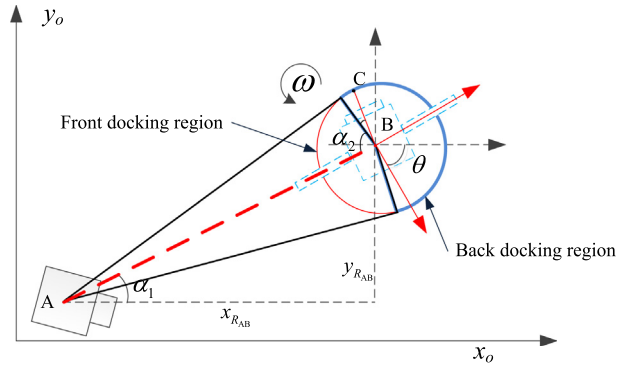

Fig. 3. Schematic of secure docking region.

it is an optimal energy trajectory. Since the docking trajectory is a function of the final time t_f and the rotation angle velocity of target is known, the preselected docking point depends on the final time t_f. When the preselected time t_f satisfies that docking point C at time t_f is in the front docking region, the docking process is secure. In the front docking region, based on the geometrical relationship, the rotation range of point C satisfies

$$\theta_0+\alpha_1-\alpha_2+2k\pi\leqslant\Delta\theta\leqslant\theta_0+\alpha_1+\alpha_2+2k\pi\quad k=0,1,2\ldots \tag{27}$$

where $\alpha_1=\arctan\frac{y_{R_{AB}}}{x_{R_{AB}}}$, $\alpha_2=\arccos\frac{R}{R_{AB}}$. So the final time t_f satisfies

$$\frac{\theta_0+\alpha_1-\alpha_2+2k\pi}{\omega}\leqslant t_f\leqslant\frac{\theta_0+\alpha_1+\alpha_2+2k\pi}{\omega}\quad k=0,1,2\ldots \tag{28}$$

3.3. Collision avoidance with solar panels

A method for collision avoidance with solar panels using the optimal trajectory is presented here. In this method, two phases of optimal guidance are adopted. Define a radius R' as shown in Fig. 4. It includes the rotation radius of solar panels. On the circle of radius R', there is a point C'(shown in Fig. 4) which has the same rotation angle with point C. Outside the circle of radius R', the trajectory cannot encounter with the solar panel. In the first optimal trajectory, the docking target point is point C'. The final time is selected based on the inequality (28), and the optimal guidance is generated using optimal solution (15), (16), (18) and (23)–(26). When chaser reaches C′, the second optimal approach starts. To the second optimal approach, the initial position is the point C', and the docking target point is point C. The final time t_f also satisfies inequality (28). The second optimal docking must be accomplished in the first period to avoid collision with solar panels, i.e. k = 0. The period of the first trajectory is unconstrainned, $k=0,1,2\ldots$.

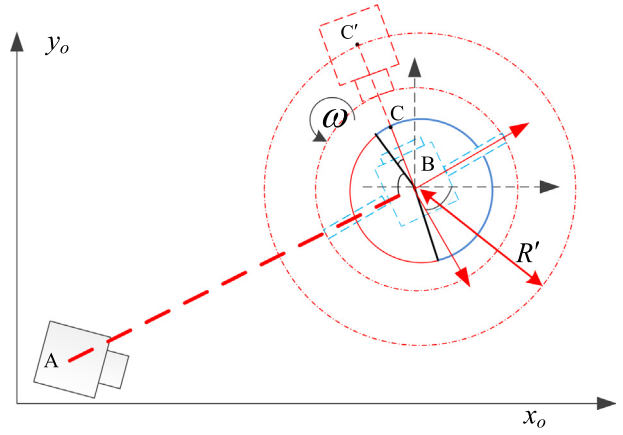

Fig. 4. Schematic of imagined docking point C′.

4. Simulation and analysis

4.1. Flying-around approach simulation

The docking guidance simulation using the method in Section 2 is shown in Fig. 5. In this simulation, the target spacecraft has an angular velocity 0.5°/s. The initial position of chaser spacecraft in the coordinate system $o_ox_oy_oz_o$ is [0, 3]; [3, 5], [6, 7] respectively. The initial position of target spacecraft in the coordinate system $o_ox_oy_oz_o$ is [8, 8] and the final docking position in $o_tx_ty_tz_t$ is [−0.8; 0]. The initial angle is $\theta_0=0$. Asterisks in this figure are the point C and A in different times. The connecting lines of asterisks represent the relative displacement between the point C and A. The relative displacement is decreasing during proximity maneuvers. The trajectories of C and A coincide after chaser spacecraft arrives at the final docking position. Trajectory of A becomes a circle curve later. Chaser spacecraft will translate around target spacecraft. However, these trajectory curves have a large curvature radius at the initial phase. With the initial relative distance increasing, the total

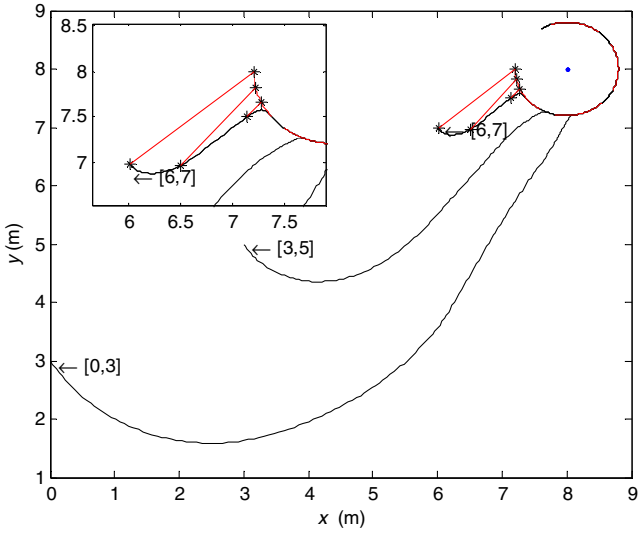

Fig. 5. Flying-around approach trajectory.

movement distance becomes longer, so more energy is consumed in the situation of longer initial relative distance.

The velocities and accelerations of docking in the initial position [6, 7] are shown in Fig. 6. It indicates that the velocity of chaser spacecraft strongly changes in the initial docking process and chaser need a violent change acceleration. Relative velocities $\boldsymbol{v}_r$ between the chaser and the docking point C in coordinate $o_o x_o y_o z_o$ are also given in left figure of Fig. 6. It indicates that the relative velocities go to zero when chaser arrives docking point C. From Fig. 6 we know, at the initial time, the chaser has an initial velocity in coordinate $o_o x_o y_o z_o$. This is because the chaser needs a synchronous rotation velocity to follow the target spacecraft. Therefore, the initial velocity of chaser needs to be established to track the flying-around approach trajectory. The method of optimal energy guidance can establish the initial state for the flying-around approach and will be discussed in next section.

The angle and angular velocity of chaser and target, relative angle and relative angle velocity during docking process are shown in Fig. 7. Relative angle θ_{tc} and relative angle velocity $\dot{\theta}_{tc}$ (red dash-dot line in Fig. 7) becomes zero in the end, and angular velocity ω_c is equal to ω_t. Then chaser and target rotate synchronously.

The rotation matrix C_{ot} can be updated by measuring rotation angle of target spacecraft, or estimating the rotation angle based on dynamics of target spacecraft. The position and rotation angular velocity of target spacecraft can be varying. A proximity trajectory, when target spacecraft has a velocity $v_t = [0.01, 0]$ and two spacecraft have a relative velocity $[0.02, -0.01]$, is shown in Fig. 8. It indicates that flying-around approach method can be used for the condition that target spacecraft moves and relative velocity exists in the initial time.

Proximity trajectories of different angular velocities of target spacecraft (initial position is [6, 7]) are shown in Fig. 9. Though in these trajectories chaser spacecraft can approach the target spacecraft and maintain the relative positions after chaser arrives at docking positon, the proximity trajectory have a large curvature radius which indicates much energy is needed in this process. The proximity trajectory of angular velocity 5°/s in Fig. 9 verifies this.

Flying-around approach method is obtained by inverse dynamics and coordinate transformation from body-fixed coordinate system $o_t x_t y_t z_t$ to orbital coordinate system $o_o x_o y_o z_o$. Even though the positon and angular velocity of the target spacecraft may change, the proximity trajectory and guidance law can be obtained as long as the positon and angular velocity of target can be measured. After reaching the docking position, chaser spacecraft continues tracking the flying-around approach trajectory and can maintain the relative position to target spacecraft. But long initial relative distance and large rotation angular velocity of target spacecraft may lead to high energy consumption. So flying-around approach method is appropriate for condition of low rotation rates and short relative distance. In addition, flying-around approach method indicates that an initial fly-around velocity of chaser must exist (as shown in Fig. 6). So a method that establishes an initial velocity for chaser spacecraft is needed to be discussed.

4.2. Optimal energy guidance simulation

A series of trajectories using optimal energy guidance of different final time t_f are shown in Fig. 10. The initial position of chaser spacecraft and target spacecraft are [8, 8] and [0, 3]. The angular velocity of target is 0.5°/s. The initial rotation angle is $\theta_0 = \pi/4$.

The cost of optimal trajectory is $J = 4.7607 \times 10^{-4}$, $J = 5.3437 \times 10^{-5}$, $J = 1.5065 \times 10^{-5}$, $J = 7.3465 \times 10^{-6}$ and $J = 5.0240 \times 10^{-6}$, when the final time t_f is 100 s, 200 s, 300 s, 400 s and 500 s. With final time t_f increasing, the needed velocity and acceleration reduces, so the energy decreases. In Fig. 9, the angular velocity of target spacecraft is low, and velocity of point C is slow. So chaser

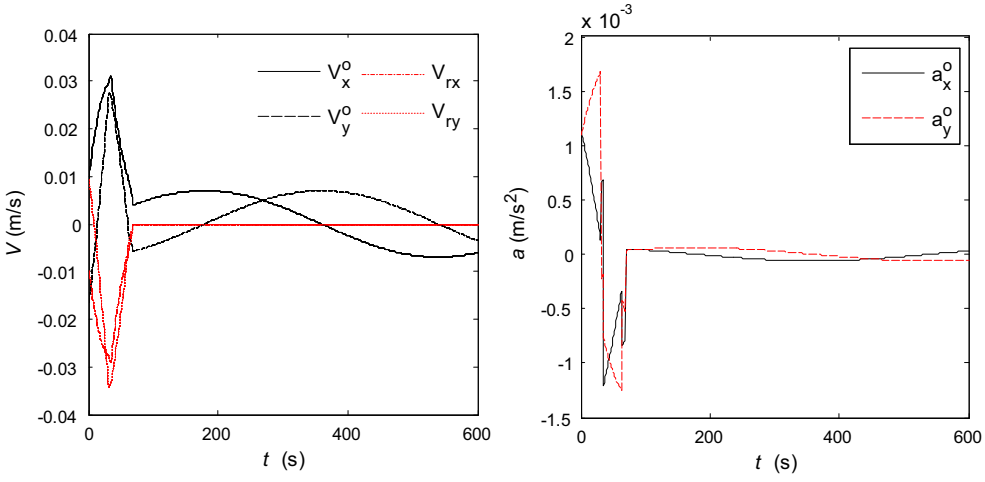

Fig. 6. Velocity, relative velocity and acceleration.

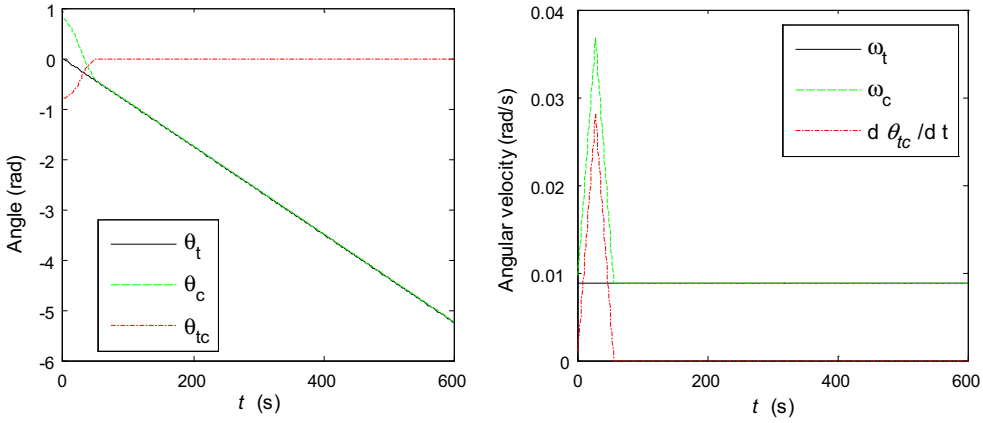

Fig. 7. Rotation angle and angular velocity.

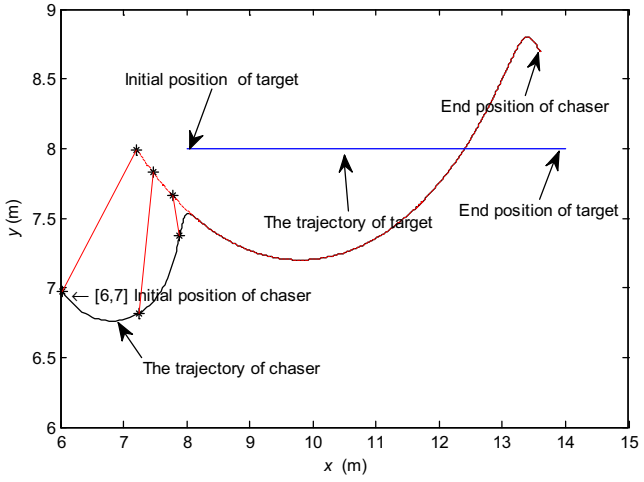

Fig. 8. Proximity trajectory when target's velocity is not zero.

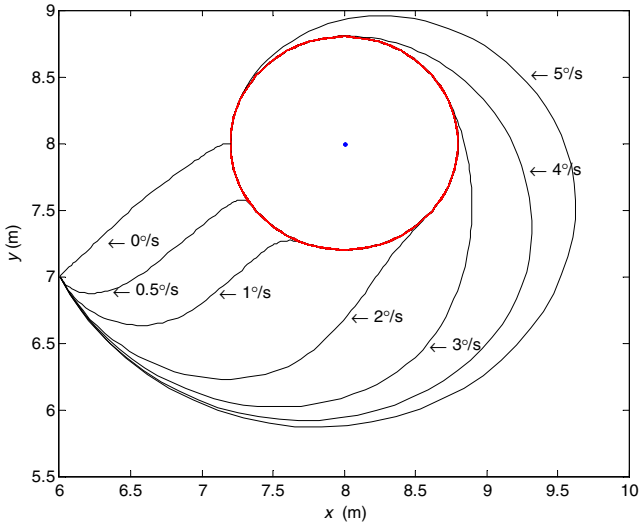

Fig. 9. Proximity trajectories in different angular velocities.

spacecraft adjusts its position and velocity only when chaser spacecraft has moved near the docking positon. Comparing with Fig. 5, the trajectory of optimal guidance

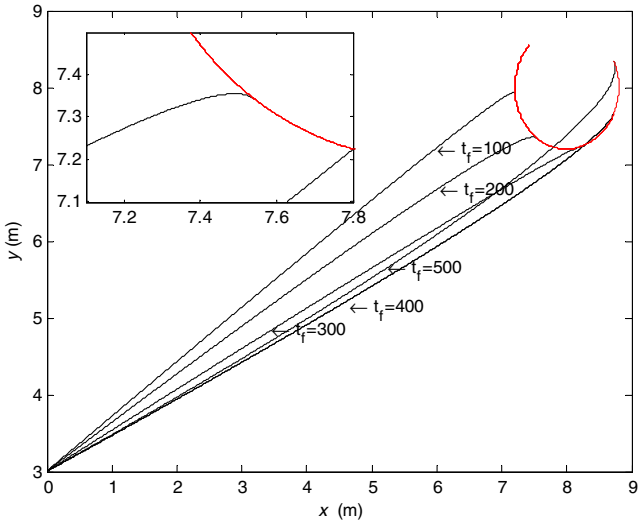

Fig. 10. Proximity trajectory.

has less radian than that of flying-around approach method. Two trajectories, whose final time 400 s and 500 s exceed the front docking region [−16.2602, 324.2817] in the first period, intersect the circle trajectory of point C. Along these two trajectories, a collision may occur between chaser spacecraft and target spacecraft. So these two trajectories are unacceptable. The final time decides whether the trajectory can be adopted.

Adding the rotation angular velocity of target to 2°/s, the initial rotation angle is also $\theta_0 = \pi/4$. The final time based on the inequality (28) should satisfy

$$-4.0651 + 180k \leqslant t_f \leqslant 81.0704 + 180k \quad k = 0, 1, 2 \ldots \tag{29}$$

where 180 is the rotation period. The lower limit −4.0651 indicates that the initial rotation angle $\pi/4$ is in the front docking region. Several trajectories in the first period (t_f is 30 s, 50 s, 100 s) and those in same docking position of different periods (50 s + 180k, k = 0, 1, 2) are shown in Fig. 11. Trajectories in front docking region do not

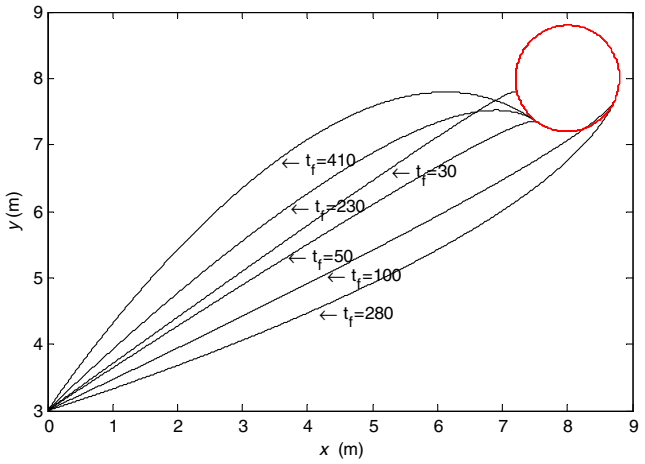

Fig. 11. Proximity trajectory when $\omega = 2°/s$.

intersect with trajectory of point C. However, the trajectory of final time 100 s which exceeds the range (29) intersects with trajectory of point C. Different period trajectories (50 s + 180k, k = 0, 1, 2) have same final docking position. When the final time increases, the trajectory radian increases and the energy decreases, as the less acceleration.

The velocities and accelerations in different periods are shown in Fig. 12. They have the same terminal velocities, but have different maximum velocity and acceleration. The less final time trajectory has the larger velocity, so more energy is consumed for larger velocity. Compared with the flying-around approach method, the acceleration of optimal trajectory is a straight line. The acceleration changes slightly. The acceleration of longer final time has smaller slope.

The two back docking trajectories of $t_f = 100$ s or 280 s in Fig. 11 meet at the same terminal position. But the trajectory in $t_f = 100$ s intersects the trajectory of point C, and the trajectory in $t_f = 280$ s comes around the circle trajectory of point C as the optimal trajectory radian increases. Many simulations indicate that the optimal trajectory do not intersect the trajectory of point C in the front docking region. However, in the back docking region, they have the possibility to intersect. Furthermore, when the target spacecraft has solar panels, the trajectory whose docking point is in the back docking region may lead to the two spacecraft collision.

A collision-avoidance optimal trajectory is shown in Fig. 13. In this simulation the rotation angular velocity is also 2°/s. The length of solar panel is 1.5 m. The final time t_{f1} of the first trajectory satisfies

$$0.59 + 180k \leqslant t_{f1} \leqslant 76.45 + 180k \quad k = 0, 1, 2 \ldots \tag{30}$$

The final time of the first optimal trajectory (the solid line in Fig. 13) is $t_{f1} = 60s$. The terminal position of the first trajectory is [7.4, 5.8], and the terminal velocity is [0.078, −0.021], which are also the initial state of the second trajectory. The front docking range t_{f2} of the second trajectory satisfies

$$-34.82 + 180k \leqslant t_{f2} \leqslant 34.82 + 180k \quad k = 0, 1, 2 \ldots \tag{31}$$

Moving from point C' to point C in a period, $k = 0$, chaser spacecraft will not collide with solar panel. The time range of the second trajectory is symmetrically distributed about zero. In Fig. 13, the final time t_{f2} is 20 s. Eqs. (29)–(31) indicate that the time range of front docking is increased. Considering avoiding collision with the body of chaser spacecraft and solar panels, a secure range $\lambda_{max} = \pi/3$ is given. The secure lines in the two final times are shown in Fig. 13.

A phase optimal trajectory, whose final time is $t_f =$ 80 s and target position is point C, is also shown in Fig. 13. This trajectory intersects with the secure line and its docking angle of incidence is so large that it is unhelpful for docking with target spacecraft. While the trajectory including two phases of optimal trajectories comes around the secure lines and its docking angle of incidence is less. So the method using two phases of optimal guidance has better effectiveness for docking and avoiding collision. In addition, if only one optimal trajectory is adopted to approach target spacecraft, the front-docking time range is [−4.06, 81.07], and the terminal time must be in one rotation period. While the front-docking time of the two phases of optimal guidance can be 111.27 s at least. The

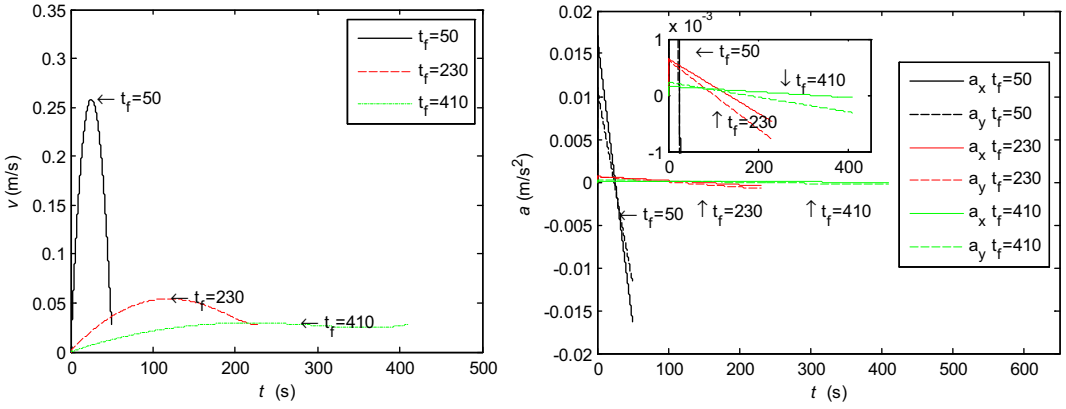

Fig. 12. Velocities and Accelerations in different periods.

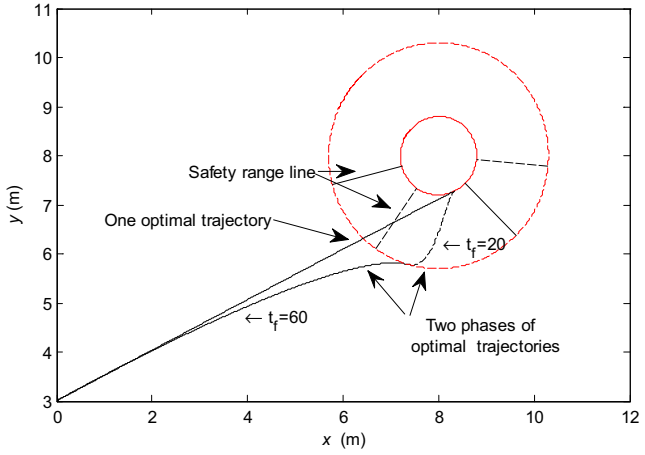

Fig. 13. Approach trajectory with collision avoidance.

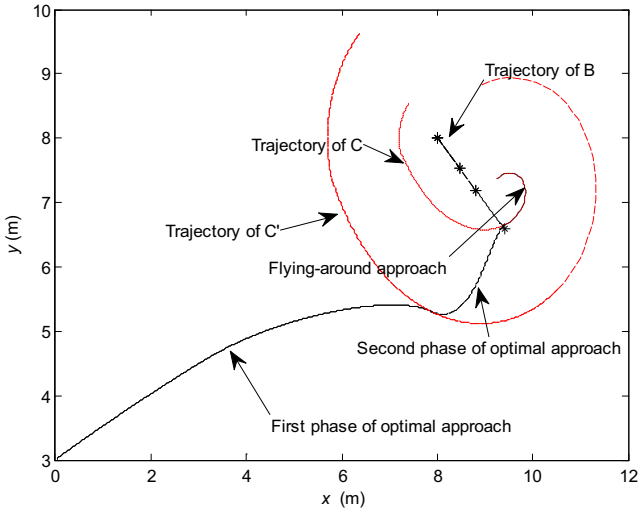

Fig. 14. Approach trajectories.

front-docking range is expanded. The first phase can also adopt different periods.

At the end of the first optimal trajectory, the chaser spacecraft has the same velocity with the point C′. Subsequently chaser spacecraft starts the second optimal trajectory tracking without waiting. After these two optimal trajectories, the relative of velocity of point A and C is zero, and the chaser spacecraft only has a tangential speed of the circle trajectory. It is just the initial velocity necessary condition of flying-around approach method. Next, flying-around approach method can be used to maintain the relative position and prepare docking with target spacecraft.

4.3. Entire docking process simulation

An entire docking maneuver of optimal energy guidance and flying-around approach method is simulated. The final time t_{f1} of the first phase is 60 s. The target angular velocity is 2°/s at initial phase. At 30 s, the target has an angular acceleration 0.05°/s^2 and a velocity [0.02, −0.02]. The final time t_{f1} is updated using Eq. (18). At the end of the first approach phase, the rotation angle velocity becomes about 3.16°/s^2. The final time t_{f1} becomes about 53 s as angular velocity changes. Then the second phase starts. The presupposed final time t_{f2} of the second phase is 20 s. After that, the flying-around approach starts. The approach trajectory is shown in Fig. 14. Velocities of chaser, point C′, point C and acceleration of chaser are shown in Figs. 15 and 16.

Using closed loop form, chaser spacecraft reaches the docking position when the target spacecraft has a varying angular rate and a non-zero velocity. Acceleration curve changes from a straight line to a curve after 30 s. At the final time t_{f1} and t_{f2}, the velocities of point A equal to that of point C′ and point C respectively, which are the combination of the linear velocity of rotation and the velocity of target spacecraft. Then the flying-around approach method can be adopted. And the terminal velocity of the second phase optimal trajectory is appropriate for the initial

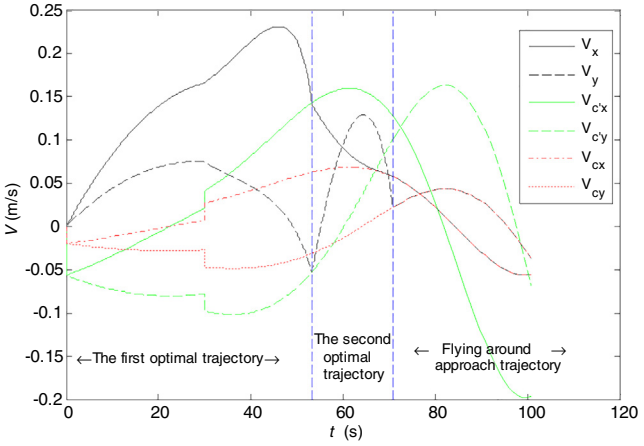

Fig. 15. Velocities.

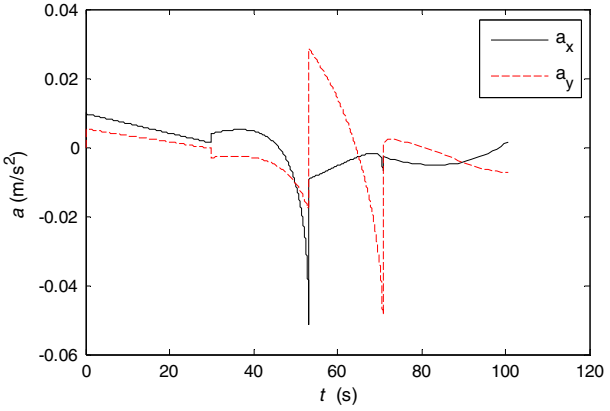

Fig. 16. Accelerations.

velocity condition of flying-around approach method. Combination of the two approach menthes, the energy is saved by optimal energy guidance method and stable docking position is provided by flying-around approach method.

5. Conclusion

This paper presents a method to solve the approach guidance problem for docking with the rotating target spacecraft. This method includes flying-around approach method and optimal energy guidance method. Flying-around approach method can arrive at the docking position and maintain a fixed relative position and relative attitude to rotating target. Unfortunately, flying-around approach method consumes much energy, and is inefficient for the condition of far initial relative distance and large rotation angular velocity. Also an initial velocity is needed. So the optimal energy guidance algorithm is presented next. The solution of optimal energy guidance is a function of final time. The analytical expression and closed-loop optimal guidance is obtained and can be used in real time. Front docking region is selected to avoid collision with rotating target body. The method, which combines two phases of optimal guidance, avoids collision with solar panel, expands the front docking range, and has better angle of incidence for docking. The terminal state is appropriate for the following flying-around approach process. Simulations indicate that combining the optimal energy guidance method and flying-around approach method, the energy can be saved and stable relative position can be provided.

Appendix A. Strategy for relative motion

The strategy for relative motion in target body-fixed coordinate system $o_t x_t y_t z_t$ is given in this appendix. An expected constant relative acceleration or relative angular acceleration a_r is determined based on the ratio of thrust to mass of chaser. A constant acceleration is beneficial to the propulsion system. The motion of 'acceleration-constant velocity-deceleration (ACD)', 'acceleration-deceleration (AD)' and 'deceleration motion (DM)' in $o_t x_t y_t z_t$ is generated based on a_r. The relative velocities of the three processes in the end are zero. Eqs. (32)–(35) give the expression of deviation Δs and the relative acceleration in the process ACD AD and DM, which are a function of time t. A maximum speed $v_{\max}$ is defined based on the energy saving principle. The spacecraft have a small initial relative velocity $v_0 (v_0 < v_{\max})$. The negative and positive relative deviations are similar in description. The positive relative deviation is discussed as follows.

When the relative deviation $\Delta s(\Lambda x, \Lambda y, \theta_{ct}) > \frac{2v_{\max}^2 - v_0^2}{2a_r}$, the relative motion is a ACD process. The chaser moves with acceleration a_r in the initial phase. When chaser reach a relative velocity $v_{\max}$, the relative acceleration becomes zero and chaser hold the relative velocity $v_{\max}$ for some distance. When the time t satisfies the third equation in Eq. (32), the relative acceleration becomes - a_r and chaser has a deceleration motion. Until the whole motion distance equals to the initial relative deviation Δs, the relative velocity and the relative acceleration become zero simultaneouslyas the fourth equation.

$$
\begin{array}{lll}
t \leqslant \frac{v_{\max}-v_0}{a_r} & s(t) = v_0 t + \frac{a_r t^2}{2} & a(t) = a_r \\
\frac{v_{\max}-v_0}{a_r} \leqslant t \leqslant \frac{\Delta s}{v_{\max}} + \frac{v_0^2}{2a_r v_{\max}} - \frac{v_0}{a_r} & s(t) = v_{\max}\left(t - \frac{v_{\max}-v_0}{a_r}\right) + \frac{v_{\max}^2 - v_0^2}{2a_r} & a(t) = 0 \\
\frac{\Delta s}{v_{\max}} + \frac{v_0^2}{2a_r v_{\max}} - \frac{v_0}{a_r} \leqslant t \leqslant \frac{\Delta s}{v_{\max}} + \frac{v_0^2}{2a_r v_{\max}} + \frac{v_{\max}-v_0}{a_r} & s(t) = \Delta s - \frac{a_r}{2}\left(\frac{\Delta s}{v_{\max}} + \frac{v_0^2}{2a_r v_{\max}} + \frac{v_{\max}-v_0}{a_r} - t\right)^2 & a(t) = -a_r \\
t > \frac{\Delta s}{v_{\max}} + \frac{v_0^2}{2a_r v_{\max}} + \frac{v_{\max}-v_0}{a_r} & s(t) = \Delta s & a(t) = 0
\end{array}
\tag{32}
$$

After this process, the relative acceleration and velocity are zero, the relative deviation holds constant. When the relative deviation $\frac{v_0^2}{2a_r} < \Delta s < \frac{2v_{\max}^2 - v_0^2}{2a_r}$, the relative motion is an AD process. The chaser will accelerate firstly, and then slow down. At last, the relative acceleration becomes zero.

$$
\begin{array}{lll}
t \leqslant \frac{\sqrt{\frac{2a_r\Delta s + v_0^2}{2}} - v_0}{a_r} & s(t) = v_0 t + \frac{a_r t^2}{2} & a(t) = a_r \\
\frac{\sqrt{\frac{2a_r\Delta s + v_0^2}{2}} - v_0}{a_r} \leqslant t \leqslant \frac{2\sqrt{\frac{2a_r\Delta s + v_0^2}{2}} - v_0}{a_r} & s(t) = \Delta s - \frac{a_r}{2}\left(\left(2\sqrt{\frac{2a_r\Delta s + v_0^2}{2}} - v_0\right)/a_r - t\right)^2 & a(t) = -a_r \\
t > \frac{2\sqrt{\frac{2a_r\Delta s + v_0^2}{2}} - v_0}{a_r} & s(t) = \Delta s & a(t) = 0
\end{array}
\tag{33}
$$

When the relative deviation $\frac{v_0^2}{2a_r} > \Delta s$, using the given acceleration a_r, chaser spacecraft arrive the target location and the relative velocity have not been decreased to zero. So a bigger acceleration or an overshoot is necessary to adjust the relative velocity. In docking process, the overshoot is impracticable. So the displacement and the relative acceleration is Eqs. (34) and (35).

When the relative deviation $\frac{v_0^2}{2a_r} > \Delta s$ and $v_0\Delta s > 0$, the relative motion is a DM process. Chaser spacecraft has a deceleration motion until the velocity is zero.

$$\begin{array}{lll} t \leqslant \frac{2\Delta s}{v_0} & s(t) = v_0 t + \frac{1}{2}at^2 & a(t) = -\frac{v_0^2}{2\Delta s} \\ t > \frac{2\Delta s}{v_0} & s(t) = \Delta s & a(t) = 0 \end{array} \tag{34}$$

When the relative deviation $\frac{v_0^2}{2a_r} > \Delta s$ and $v_0\Delta s < 0$, an AD process is adopted.

$$\begin{array}{lll} t \leqslant \left|\frac{2v_0}{a_r}\right| & s(t) = v_0 t + \frac{1}{2}a_r t^2 & a(t) = a_r \\ \left|\frac{2v_0}{a_r}\right| < t \leqslant \left|\frac{2v_0}{a_r}\right| + \left|\frac{2\Delta s}{v_0}\right| & s(t) = \Delta s + \frac{1}{2}a\left(\left|\frac{2v_0}{a_r}\right| + \left|\frac{2\Delta s}{v_0}\right| - t\right)^2 & a(t) = -\frac{v_0^2}{2\Delta s} \\ t > \left|\frac{2v_0}{a_r}\right| + \left|\frac{2\Delta s}{v_0}\right| & s(t) = \Delta s & a(t) = 0 \end{array} \tag{35}$$

References

Bevilacqua, R., Hall, J.S., Horning, J., et al., 2009. Ad hoc wireless networking and shared computation for autonomous multirobot systems. J. Aerospace Comput., Inform., Commun. 6 (5), 328–353.

Bevilacqua, R., Caprari, A., Hall, J., et al., 2009. Laboratory experimentation of multiple spacecraft autonomous assembly. In: AIAA Guidance, Navigation, and Control Conference, p. 6290.

Bevilacqua, R., Lehmann, T., Romano, M., 2011. Development and experimentation of LQR/APF guidance and control for autonomous proximity maneuvers of multiple spacecraft. Acta Astronaut. 68 (7), 1260–1275.

Boyarko, G., Yakimenko, O., Romano, M., 2011. Optimal rendezvous trajectories of a controlled spacecraft and a tumbling object. J. Guid., Control, Dyn. 34 (4), 1239–1252.

Chu, X., Zhang, J., Lu, S., et al., 2016. Optimised collision avoidance for an ultra-close rendezvous with a failed satellite based on the Gauss pseudospectral method. Acta Astronaut. 128, 363–376.

Ciarcià, M., Romano, M., 2012. Suboptimal guidance for orbital proximity maneuver with path constraints capability. Proceedings of the AIAA Guidance Navigation and Control Conference.

Ciarcià, M., Grompone, A., Romano, M., 2014. A near-optimal guidance for cooperative docking maneuvers. Acta Astronaut. 102, 367–377.

Curti, F., Romano, M., Bevilacqua, R., 2010. Lyapunov-based thrusters' selection for spacecraft control: analysis and experimentation. J. Guid., Control, Dyn. 33 (4), 1143–1160.

Hakima, H., Bazzocchi, M.C.F., Emami, M.R., 2018. A deorbiter CubeSat for active orbital debris removal. Adv. Space Res. 61 (9), 2377–2392.

Jewison, C.M., McCarthy, B., Sternberg, D.C., et al., 2014. Resource aggregated reconfigurable control and risk-allocative path planning for on-orbit servicing and assembly of satellites. In: AIAA Guidance, Navigation, and Control Conference, p. 1289.

Ma, Z., Ma, O., Shashikanth, B.N., 2006. Optimal control for spacecraft to rendezvous with a tumbling satellite in a close range. In: Intelligent Robots and Systems, 2006 IEEE/RSJ International Conference on. IEEE, pp. 4109–4114.

McCamish, S.B., Romano, M., Nolet, S., et al., 2009. Flight testing of multiple-spacecraft control on SPHERES during close-proximity operations. J. Spacecraft Rockets 46 (6), 1202–1213.

Mohan, S., Sakamoto, H., Miller, D.W., 2007. Formation control and reconfiguration through synthetic imaging formation flying testbed (SIFFT). Optical Engineering+ Applications. International Society for Optics and Photonics, 66871E-66871E-11.

Nolet, S., Miller, D.W., 2007. Autonomous docking experiments using the SPHERES testbed inside the ISS. Sens. Syst. Space Appl. 6555 (1), 65550P.

Pellegrini, V., Bevilacqua, R., Romano, M., et al., 2010. Spacecraft proximity navigation and autonomous assembly based on augmented state estimation: analysis and experiments. Proceedings of the AIAA Guidance, Navigation, and Control Conference.

Romano, M., Friedman, D.A., Shay, T.J., 2007. Laboratory experimentation of autonomous spacecraft approach and docking to a collaborative target. J. Spacecraft Rockets 44 (1), 164–173.

Scharf, D.P., Keim, J.A., Hadaegh, F.Y., 2010b. Flight-like ground demonstrations of precision maneuvers for spacecraft formations—Part II. Syst. J., IEEE 4 (1), 96–106.

Scharf, D.P., Keim, J.A., Hadaegh, F.Y., 2010a. Flight-like ground demonstrations of precision maneuvers for spacecraft formations—part I. Syst. J., IEEE 4 (1), 84–95.

Sternberg, D.C., 2017. Optimal Docking to Tumbling Objects with Uncertain Properties. Massachusetts Institute of Technology.

Sternberg, D., 2018. Multiple model trajectory generation for uncertain target spin direction. In: 2018 IEEE Aerospace Conference. IEEE, pp. 1–12.

Sternberg, D., Miller, D., 2017. Mapping a chaser satellite's feasibility space for soft docking. In: Aerospace Conference, 2017 IEEE. IEEE, pp. 1–12.

Sternberg, D.C., Miller, D., 2018. Parameterization of fuel-optimal synchronous approach trajectories to tumbling targets. Front. Robot. AI 5, 33.

Sun, L., Zheng, Z., 2017. Adaptive relative pose control for autonomous spacecraft rendezvous and proximity operations with thrust misalignment and model uncertainties. Adv. Space Res. 59 (7), 1861–1871.

Wilde, M., Ciarcià, M., Grompone, A., et al., 2016. Experimental characterization of inverse dynamics guidance in docking with a rotating target. J. Guid., Control, Dyn., 1173–1187

Wu, Y., Han, F., Zheng, M., et al., 2018. Attitude control for on-orbit servicing spacecraft using hybrid actuator. Adv. Space Res. 61 (6), 1600–1616.